Sensors and Materials, Vol. 38, No. 6 (2026) 3457–3470
MYU Tokyo

S & M 4513

GPS Surface Drifter System for Scale-dependent Horizontal Diffusivity Estimation in the Northwestern Pacific Ocean

Seongbong Seo,[1] Kyeong Ok Kim,[1] Young-Gyu Park,[1] and Jun Myoung Choi[2*]

[1]Ocean Circulation and Climate Research Department, Korea Institute of Ocean Science and Technology (KIOST), Busan 49111, South Korea
[2]Department of Ocean Engineering, Pukyong National University, Busan 48513, South Korea

(Received November 24, 2025; accepted June 11, 2026)

Keywords: surface drifter, horizontal diffusivity, relative dispersion, pair statistics, northwestern Pacific Ocean

Scale-dependent horizontal diffusivity at the sea surface is a controlling parameter for the trajectory and dilution of soluble pollutants and other tracers. A lightweight, low-cost GPS surface drifter with satellite telemetry, a durable low-profile hull, and a sustained operational lifetime of around two months has been developed, enabling cluster-style releases for pair statistics across a wide range of separation scales. Nineteen units were deployed from research vessel (R/V) Isabu during August and October 2024 at two energetic sites in the seas of the western Pacific and south of Japan. Relative dispersion from the trajectories yields scale-dependent diffusivity that rises from the order of 10^1 m^2s^{-1} at 10 km to 10^3 m^2s^{-1} near 100 km, with values of 2.7×10^1 and 9.6×10^2 m^2s^{-1} for the western Pacific site and 4.3×10^1 and 1.7×10^3 m^2s^{-1} for the region south of Japan. The empirically constrained curve for horizontal diffusivity as a function of scale provides a direct constraint for subgrid-scale mixing in coarse-resolution contaminant transport models and demonstrates the field readiness of the new drifter system.

1. Introduction

Ocean pollutants introduced at the sea surface can spread over basin scales. Predictive skill in hazard and resource applications, such as tracking contaminants or debris, depends on how horizontal mixing is represented in the surface layer where lateral stirring is strongest.(1) Quantitatively understanding the horizontal dispersion mechanism at the ocean surface, where these pollutants are concentrated, is therefore paramount for impact assessment and mitigation strategies.

Ocean models are key tools utilized in predicting the trajectories and concentration distributions of pollutants.(2) The accuracy of these computational models, however, is fundamentally limited by the horizontal grid resolution. Motions below the grid scale that the model cannot explicitly resolve must be represented through parameterization.(3,4) This parameterization for horizontal mixing is traditionally based on a gradient-diffusion model,

*Corresponding author: e-mail: jmchoi@pknu.ac.kr
https://doi.org/10.18494/SAM6206

ISSN 0914-4935
https://myukk.org/

where horizontal diffusivity (K_h) is determined. A fundamental weakness of many existing models is the assumption that K_h is a constant or spatially uniform value, regardless of region or scale.[4,5]

The assumption of constant diffusivity is problematic because sub-mesoscale (0.1–10 km) eddies and fronts play a dominant role in horizontal mixing in the upper ocean.[6] High-resolution modeling results clearly demonstrate the importance of resolving these scales. Ntaganou *et al*.[7] compared a 4 km model with a 1 km model in the Gulf of Mexico. The 1 km simulation produced more vigorous mixing and higher separation rates, leading to a more realistic prediction of particle dispersion. Similar results were confirmed in case studies following the Fukushima Daiichi Nuclear Power Plant accident, where applying a high-resolution downscaling technique showed that the sub-mesoscale effect enhanced both horizontal and vertical mixing, contributing significantly to 3D tracer variability.[8] The results of these studies imply that high horizontal resolution is essential to successfully implement 3D dispersion in coastal regions.

Performing long-term global pollutant distribution predictions at a resolution of 1 km or more can require significant computational resources. A 100-km-grid global model must parameterize all mixing below 100 km as the subgrid scale, while a 10-km-grid regional model must parameterize processes below 10 km. These two models physically require different K_h values. In real ocean turbulence, K_h is not constant but is scale-dependent.[9,10] The mixing efficiencies at the 1 km and 100 km scales are physically different, and their K_h values can differ by orders of magnitude. This implies that scale-aware parameterization, which defines K_h as a function of scale L, is essential.[5] To achieve this, the $K_h(L)$ relationship must be empirically measured through field observations.

The most direct and powerful method to measure $K_h(L)$ in the field is by using Lagrangian surface drifters that follow the movement of the water.[11,12] The classical single-particle statistics methodology based on Taylor[13] is limited because the resulting 'absolute dispersion' can be contaminated by large-scale mean flow and shear dispersion.[14] To isolate the pure turbulent mixing component needed for subgrid-scale parameterization, Batchelor[15] proposed pair statistics, which measure the relative dispersion (D^2) of drifter pairs. This methodology removes the influence of the mean flow acting commonly on both particles and naturally quantifies the scale dependence of K_h by using the drifter pair separation (D) itself as the scale variable.[16]

The pair-statistics methodology, however, presents a significant technical bottleneck. To obtain reliable statistics, a sufficient number of drifter pairs is required for statistical convergence, which presupposes a high-count or massive-scale cluster release. Traditional instruments, such as the Global Drifter Program (GDP) Surface Velocity Program (SVP) drifter, are not economically suitable for such cluster studies owing to high manufacturing and satellite communication costs.[12]

This study, set against this scientific, methodological, and technical background, is aimed at ultimately improving the subgrid-scale parameterization of pollutant dispersion models. The specific objectives are threefold. First, to develop and validate a low-cost, lightweight, high-performance GPS surface drifter system, demonstrating the practical application of mobile sensor technologies and durable hull materials optimized for large-scale cluster deployment and

high-frequency trajectory sampling. Second, to successfully deploy the developed system in two dynamic regions in the Northwestern Pacific Ocean, which are key pathways for pollutant transport, to acquire unique Lagrangian trajectory data. Third, to provide empirical estimates of scale-dependent horizontal diffusivity [$K_h(L)$] from the collected high-resolution pair-trajectory data, thereby contributing directly to the improvement of subgrid-scale parameterization in dispersion models.[17]

2. Data and Methods

To estimate scale-dependent horizontal diffusivity from Lagrangian observations, we employed a custom-designed low-cost drifter system and specific cluster deployment strategies. The subsequent analysis utilizes pair statistics to quantify the relative dispersion of these drifters.

2.1 Low-cost GPS surface drifter

A GPS surface drifter optimized for large-scale cluster deployment and high-frequency sampling was developed. The drifter is a cylindrical buoy 30 cm in length and 11 cm in diameter with an ultralight weight of approximately 500 g (Fig. 1). This ultralight, compact design allows a single researcher to rapidly deploy multiple units simultaneously from the research vessel deck, enabling cluster deployment. Communication is via the Globalstar satellite network. The raw GPS fixes were initially recorded at 5 min intervals. To regularize occasional missing records, a 15 min analysis grid was generated through piecewise cubic Hermite interpolation (PCHIP).

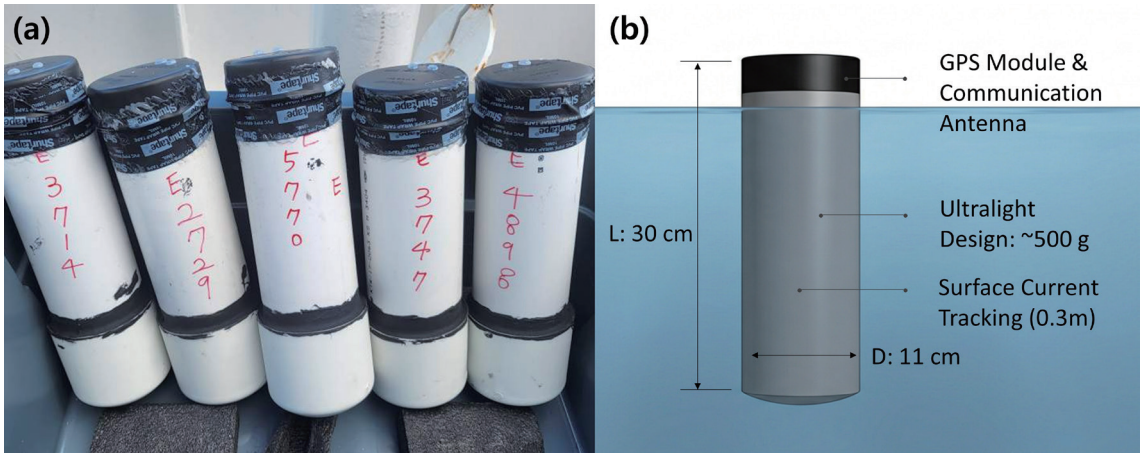

Fig. 1. (Color online) (a) Photograph of the GPS surface drifter prototype and (b) schematic diagram of the drifter's surface-following design.

Furthermore, by modifying the power supply into two parallel strings of four D-cell batteries, the total capacity was substantially increased, allowing the drifters to operate stably for more than 30 days in the field. While other modern communication systems such as Iridium also provide high-precision location [*O* (1.5 m)], the Globalstar system was selected for its high-frequency sampling and affordable flat-rate data plans, which maximize the economic feasibility of large-scale deployments for sub-mesoscale research.

The drifter has a drogueless, surface-following design to directly mimic the horizontal dispersion of dissolved pollutants mixed in the uppermost layer of the ocean. The cylindrical hull is designed to remain almost entirely submerged, leaving only the communication module above the sea surface. This low-profile configuration reduces, but does not completely eliminate, direct windage drag, allowing the drifter to effectively track the currents in the uppermost layer (upper 0.3 m) rather than being driven primarily by wind. This design contrasts with the 15-m-drogue SVP drifters designed to follow mixed-layer currents,[12] but the system was engineered to align with the low-cost, lightweight, large-scale cluster deployment.[18]

The developed system was deployed in two key regions of the Northwestern Pacific using the research vessel (R/V) Isabu (Fig. 2). The first deployment was in the Western Pacific (WP) on

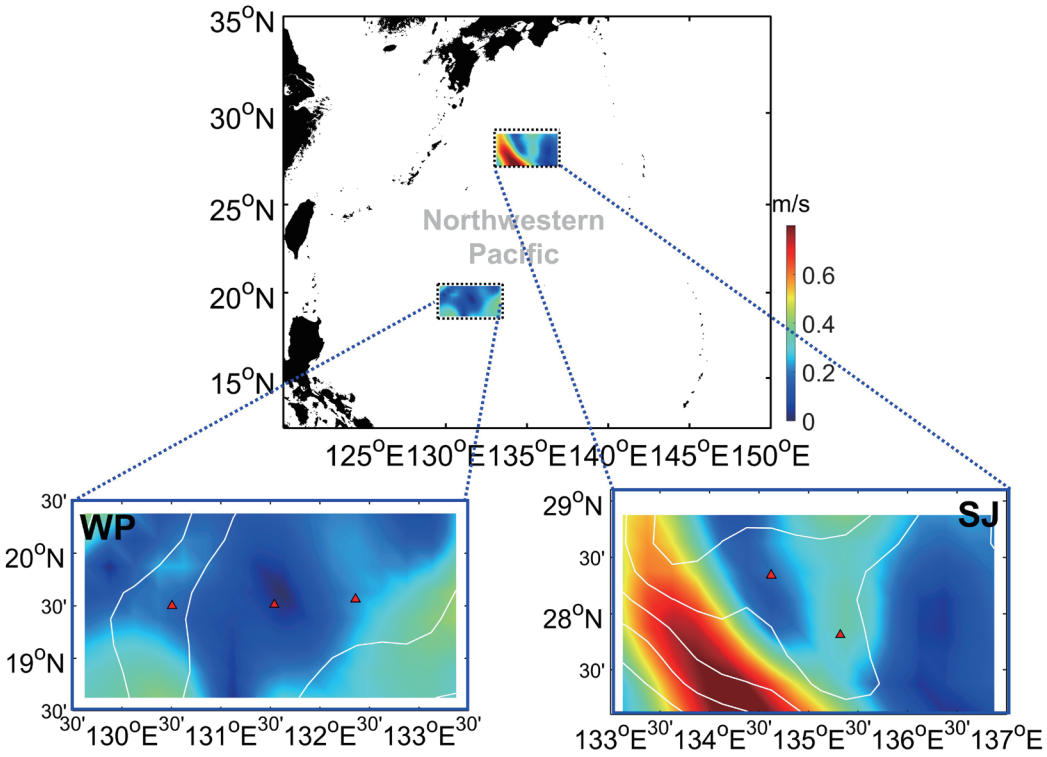

Fig. 2. (Color online) Study area and deployment geometry. Western Pacific (WP) and south of Japan (SJ) clusters are shown together with geostrophic currents (supplied by Copernicus Marine Service; https://doi.org/10.48670/moi-00148) that influence the sites at the time of deployment.

24 August 2024, where nine drifters were deployed in three groups. The WP region is an eddy-rich zone with high eddy kinetic energy in the Northwest Pacific. The second deployment was south of Japan (SJ) on 24 October 2024, where 10 drifters were deployed in two groups of five. This region is a complex region influenced by recirculation south of the Kuroshio Current, which is characterized by strong currents and high eddy kinetic energy.[19] A pair- and triplet-based deployment and grouped deployment strategies were adopted to secure a large number of drifter pairs with very small initial separation distances, allowing for a statistically significant analysis of the small-scale dependence of K_h.[20]

2.2 Pair statistics

Pair statistics were used to quantify surface dispersion in terms of the growth of separation between nearby drifters. Positions from each cluster were available every 15 min for the full deployment period. Raw trajectories were first subjected to quality control by removing obvious outliers and short gaps. After this step, each drifter track consisted of a sequence of positions, $(x_i(t), y_i(t))$ at times t_k measured in days from the first observation in each deployment. The analysis focused on horizontal separation within the local tangent plane. Geographic coordinates were converted to metric east–north coordinates using a Universal Transverse Mercator (UTM) projection, which avoids distortion over the limited spatial extent of each cluster and simplifies the computation of distances.[21]

Pairs were selected at an initial reference time when the interdrifter distance was below a threshold r_0. A value of $r_0 = 500$ m was adopted in both regions, which is small compared with the target separation range from 10 to 100 km yet large enough to retain a sufficient number of pairs. For every cluster and every reference time, all unique drifter combinations, (i, j), that satisfied $0 < D_{ij}(t_0) < r_0$ were included, where the instantaneous separation is

$$D_{ij}^2(t) = \left[x_i(t) - x_j(t)\right]^2 + \left[y_i(t) - y_j(t)\right]^2. \tag{1}$$

Here, i and j denote drifter identifiers and k is the time index. Pairs were followed forward in time as long as both members of the pair reported valid positions. When either drifter left the domain or the record ended, the corresponding pair was removed from the statistics. The procedure produced an ensemble of separations, $D_{ij}(t)$, and a time-dependent number of active pairs, $N_{pair}(t)$, for each region.

Relative dispersion was defined as the mean square separation over all active pairs,

$$\left\langle D^2(t)\right\rangle = 1/N_{pair}(t)\sum_{i<j} D_{ij}^2(t), \tag{2}$$

where the angle brackets denote an ensemble average at a fixed time. The initial value of $\langle D^2(t_0)\rangle$ was close to r_0^2 and much smaller than the values reached later in the record. For visualization

and comparison with earlier work, relative dispersion was plotted in units of km^2 as a function of elapsed time in days on log–log axes, together with a reference slope proportional to t^3 that represents a classical Richardson regime. The number of active pairs, $N_{pair}(t)$, was plotted on a separate panel to document the degree of statistical support for the dispersion estimate at each time.

The pair selection and time-stepping procedure involved searching all drifters in the cluster at every analysis time, constructing the set of pairs with initial separation below r_0, and storing the distance time series for each pair. This process returned the mean square separation $\langle D^2(t_0)\rangle$, its zonal and meridional components, the number of active pairs, and the corresponding time vector. The time step in the analysis was kept equal to the sampling interval of 15 min, and the final curves were smoothed only through averaging over many pairs, not through any additional time filtering. As a result, the early part of the record retained the imprint of high-frequency motions such as inertial oscillations and short surface waves. Because the nominal positional error of the drifters (~5 m) is much smaller than the typical displacement over a 15 min interval, these high-frequency fluctuations are regarded as physically meaningful components of near-surface motion rather than instrumental noise.

Scale-dependent horizontal diffusivity was evaluated from the growth rate of the mean square separation. Following the general framework of Batchelor[15], we estimated the effective horizontal diffusivity K_h directly from the relative dispersion $\langle D^2(t_0)\rangle$ and elapsed time t using the bulk formulation to minimize the impact of high-frequency positional fluctuations.

$$K_h(t) = \frac{\left\langle D^2(t)\right\rangle}{4t} \tag{3}$$

This bulk formulation avoids the use of instantaneous time derivatives, thereby minimizing the impact of high-frequency positional fluctuations on diffusivity estimates. For diagnostic plots that span many orders of magnitude in both time and separation, diffusivity was finally expressed as a function of separation scale rather than time. A scale coordinate was defined as

$$D(t) = \sqrt{\left\langle D^2(t)\right\rangle} \tag{4}$$

and the corresponding diffusivity values were associated with these mean separations to produce $K_h(D)$. The mapping from time to scale is one-to-one over the range where separation grows monotonically, which holds for the present deployments, so the procedure yields a well-defined function $K_h(D)$ over scales from the order of 10 km to the order of 100 km.

A logarithmic binning procedure was used to reduce scatter in both the relative dispersion and diffusivity curves as functions of separation. For each region, the sequence of pairs ($D(t)$, $K_h(t)$) was binned into twenty-four intervals that were uniformly spaced in $\log_{10}D$. This procedure grouped all samples whose separation fell within a given bin, then assigned the geometric mean of the bin edges as the representative scale and the arithmetic mean of K_h in that

bin as the representative diffusivity. Bins containing fewer than a prescribed minimum number of samples were discarded to avoid poorly constrained estimates. The resulting binned curve retained the main trend of raw estimates while suppressing the small-scale variability produced by finite sampling. The method produced a single curve $K_h(D)$ for each deployment region, which forms the main quantitative result used in the discussion of scale-dependent mixing.

3. Results and Discussion

Here, we present the observed Lagrangian trajectories from the cluster deployments and analyze the evolution of relative dispersion over time. From these statistics, scale-dependent horizontal diffusivity (K_h) is derived for each region, and its implications for subgrid-scale parameterization in ocean models are discussed.

3.1 Drifter trajectories

All nineteen units transmitted successfully for periods approaching two months (Fig. 3). The tracks in the WP region show a smooth, gradual southwestward drift with gradual spreading from the initial clusters. In sharp contrast, SJ tracks exhibit complex meanders and loops, consistent with the strong mesoscale and sub-mesoscale activities in the Kuroshio region. This contrasting trajectory structure suggests a larger diffusivity at a given scale near the SJ site.

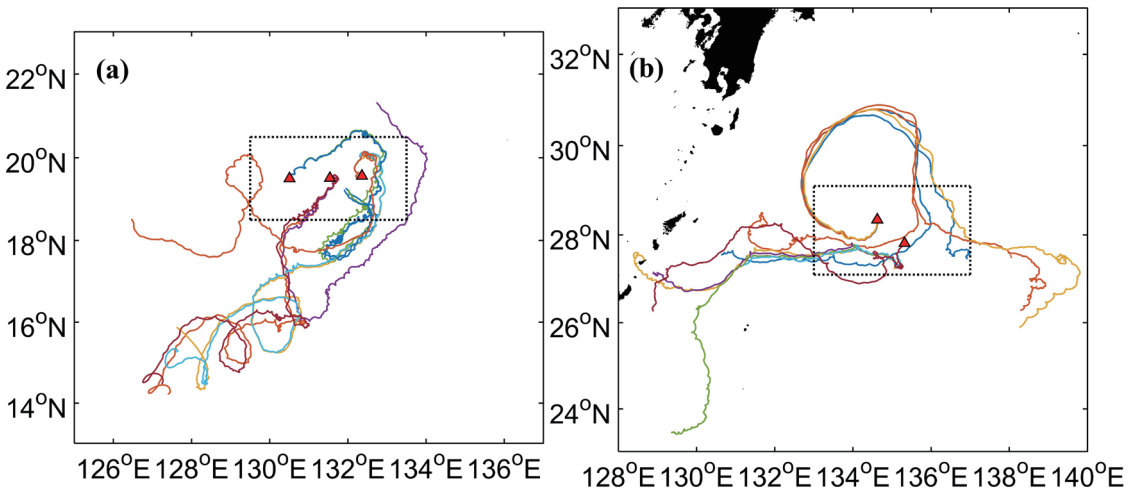

Fig. 3. (Color online) Drifter trajectories over the mission window (~2 months) for (a) WP and (b) SJ.

3.2 Relative dispersion and regime character

Relative dispersion curves for the two deployment regions reveal a vigorous spreading field that varies in intensity between sites (Fig. 4). Mean square separation grows from initial values of the order of 10^{-1} km^2 at a few hours to values exceeding 10^4 km^2 after 20 to 30 days. Separation grows more rapidly at the SJ site, but the overall shapes of the curves are similar in both regions. On log–log axes, the early stage of dispersion, over roughly the first day, shows a slope steeper than linear in time yet shallower than the ballistic (t^2) regime associated with coherent advection, which indicates that relative motion is already influenced by eddies and fronts on scales comparable to the initial spacing of the pairs.

Over intermediate times between about 1 and 10 days, the dispersion curves approach a slope close to three, which lies near the classical Richardson regime (t^3) for turbulent relative dispersion.[15] A reference line proportional to t^3 plotted alongside the data confirms that the observed curves fall within the envelope expected from geophysical turbulence theory. The approach toward a Richardson-like regime implies that pairs experience a broad spectrum of motions that transfer energy from large scales to smaller scales and that the strain field acting on the drifters is intermittent in space and time. The strong mesoscale and sub-mesoscale activities documented in western boundary current systems therefore appear in the present data as an accelerated growth of $\langle D^2 \rangle$ compared with simple diffusive spreading.

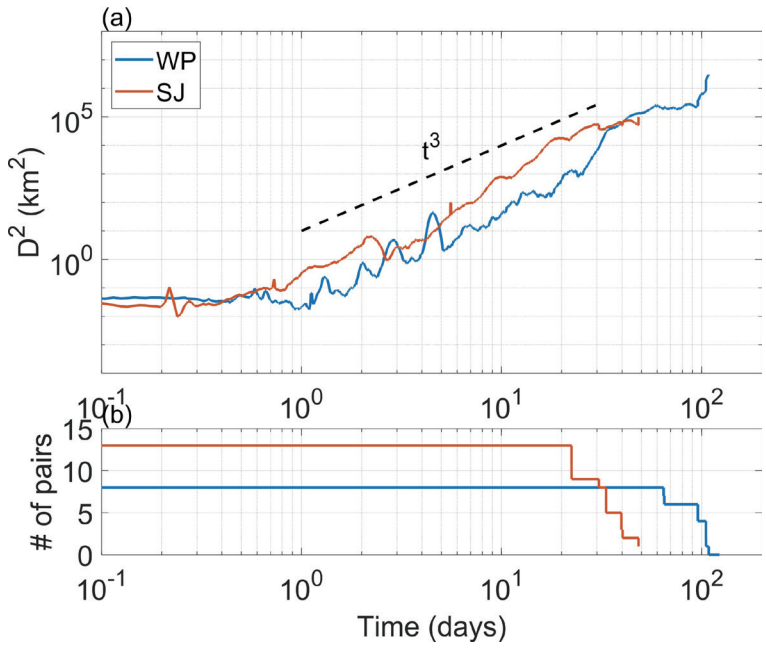

Fig. 4. (Color online) Relative dispersion and number of drifter pairs for WP and SJ drifters over time after release.

At longer times beyond 10 to 20 days, the mean square separation tends toward a lower growth rate. Part of this behavior reflects the finite size of the energetic region sampled by the drifters, since pairs eventually reach separations where one member begins to feel currents outside the core of the western boundary current jet and its adjacent eddy field. Another contribution arises from the gradual decrease in the number of active pairs as the deployment progresses. The lower panel of the distribution plot shows that the number of pairs decreases from over 10 in the first few days for SJ to less than 5 after a few weeks. For WP drifters, the initial number of pairs is less than 10, but the number of pairs remains constant for two months before decreasing thereafter. Estimates of $\langle D^2 \rangle$ at the longest elapsed times therefore rest on a smaller ensemble and display more variability between adjacent samples.

Mean square separation grows more rapidly than linearly in time even at the latest analysis times, which indicates that pairs continue to feel coherent stirring by mesoscale features. The contrast between the two regions is evident in the relative dispersion curves. The SJ curve lies above the WP curve for most of the record, which indicates stronger stirring near the Kuroshio and its upstream region. The difference is especially pronounced at intermediate times when the curves are closest to the Richardson slope, and it foreshadows a larger scale-dependent diffusivity in the Kuroshio-influenced region in the following subsection.

Although the deployment of 9 to 10 drifters per region is relatively modest, it provides a valuable first-order estimate of horizontal diffusivity. To evaluate statistical robustness, a sensitivity test was conducted by comparing K_h at $L = 100$ km using random subsets of three and six pairs. The mean relative variability was approximately 40–60% for the three-pair subsets and 25–30% for the six-pair subsets compared with the all-pair estimate. Given that horizontal diffusivity spans several orders of magnitude, this variability—remaining well within a factor of two—confirms that the overall order of magnitude and scale-dependent tendency are highly robust against finite sampling.

3.3 Scale-dependent horizontal diffusivity

The scale-dependent horizontal diffusivity estimated from the pair statistics shows a marked increase with separation scale in both regions (Fig. 5). The binned curves $K_h(D)$ rise from values near 10^1 m^2s^{-1} at separation scales of the order of 10 km to values near 10^3 m^2s^{-1} at scales approaching 100 km. The increase spans more than two orders of magnitude over roughly one decade in scale, which indicates that the efficiency of lateral stirring in the surface layer depends very strongly on the separation of the tracer patches. Such strong scale dependence contradicts the common model assumption of a constant horizontal diffusivity and highlights the need for scale-aware parameter settings in applications that seek to represent dispersion in western boundary current regions. Although sub-mesoscale motions are often associated with strong local strain rates and deformation, the effective horizontal diffusivity diagnosed at separation scale L naturally increases with L in a Richardson-type framework. Thus, a larger K_h at mesoscale separations is a physically consistent consequence of this scale dependence.

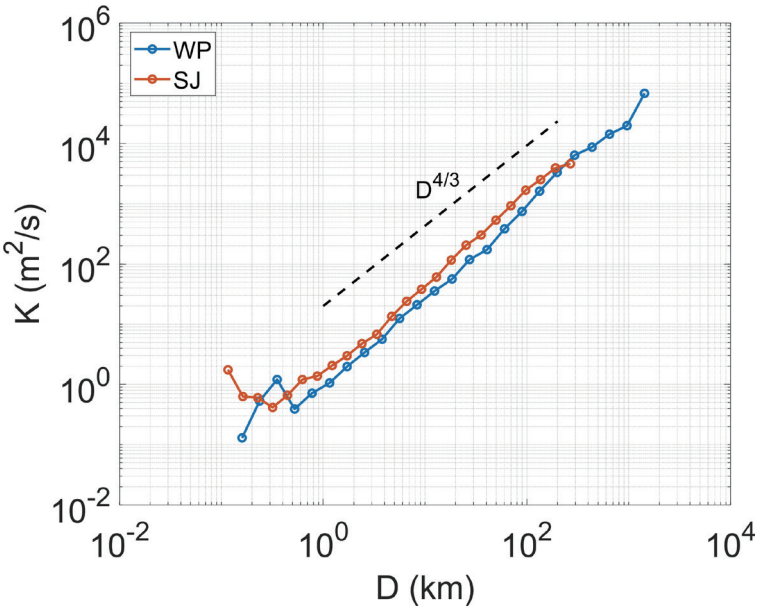

Fig. 5. (Color online) Scale-dependent horizontal diffusivity as a function of separation distance.

The curve for the WP site exhibits a relatively smooth increase of K_h with scale. At the smallest resolved scales of around 10 km, diffusivity is close to 2.7×10^1 m^{2}s^{-1} and the curve then steepens between about 20 and 50 km. Over this range, the effective slope in log–log space approaches the classical $D^{4/3}$ dependence that follows from a Richardson-type regime. A reference line proportional to $D^{4/3}$ plotted on the same axes confirms that the observed values remain within a factor of about three of this theoretical trend. At larger separations approaching 100 km, the curve begins to bend toward a gentler slope, and diffusivity values reach about 9.6×10^2 m^{2}s^{-1}.

The curve for the SJ region is consistently higher than the WP curve at small and intermediate scales. At around 10 km, K_h reaches approximately 4.3×10^1 m^{2}s^{-1}, roughly a factor of two higher than in the WP. The difference is consistent with the expectation of stronger mesoscale activity near the Kuroshio. With increasing separation, the diffusivity again follows a slope close to $D^{4/3}$ up to a scale of several tens of kilometers, then approaches values near 1.7×10^3 m^{2}s^{-1} at 100 km. At the largest scales, the two curves converge within the uncertainty implied by finite sampling, which implies that the large-scale eddy field sets a similar upper limit on diffusivity in both regions.

The magnitude of the derived diffusivities is comparable to earlier estimates for energetic western boundary current systems. Drifter-derived maps of lateral diffusivity in the Kuroshio and Gulf Stream regions report values of the order of 10^4 m^{2}s^{-1} at scales near 100 km.[16,22,23] Agreement with those independent studies in capturing such energetic scaling supports the interpretation that the present cluster deployments successfully sampled the dominant stirring processes in the surface layer. The scale-dependent curves obtained here therefore provide a physically grounded basis for specifying horizontal diffusivity in regional and basin-scale

models that cannot explicitly resolve the full cascade of motions from the sub-mesoscale to the mesoscale.

When interpreting the derived $K_h(D)$ values, it must be considered that the undrogued drifters had approximately 20% of their body exposed above the water surface. Therefore, the estimated diffusivity reflects the effective near-surface dispersion driven by the combined effects of ocean currents, direct wind drag, and wave-induced Stokes drift. Unlike standard SVP drifters drogued at 15 m depth, the present system specifically captures the uppermost surface transport, making these empirically derived K_h values highly applicable for modeling the dispersion of floating marine debris, surface oil spills, and buoyant microplastics.

4. Conclusions

The GPS drifter system developed in this study successfully achieved the technical objective, highlighting the effectiveness of combining low-cost sensor technologies with lightweight materials for oceanic applications. The high-frequency sampling at 15 min intervals was crucial for resolving the early-time separation that sets the curvature of the $K_h(D)$ curve at small scales, a capability aliased by standard 1–6 h drifter data.[24] The low unit cost made the cluster releases practical, lifting the statistical bottleneck that has traditionally hindered pair analysis.[20] Furthermore, the lightweight (500 g) hardware streamlined deck operations, allowing large clusters to be deployed rapidly. The field success across two energetic regions demonstrates the operational readiness of this system for wider use in quantifying surface transport.

The cluster deployments in the Northwestern Pacific produced the dense pair statistics required to derive the scale-dependent horizontal diffusivity $K_h(L)$. The analysis demonstrated that diffusivity is not constant but is strongly scale-dependent, rising from $O(10^1)$ m^2s^{-1} at 10 km (WP: 2.7×10^1; SJ: 4.3×10^1) to $O(10^2 - 10^3)$ m^2s^{-1} at 100 km (WP: 9.6×10^2; SJ: 1.7×10^3). This $D^{4/3}$ scaling is consistent with a turbulent Richardson regime and agrees well with prior diffusivity estimates for energetic western boundary current systems.[22,23]

The most significant contribution of this study is the empirical constraint provided for $K_h(L)$, which directly addresses the challenge of subgrid-scale parameterization. The derived $K_h(L)$ curves offer immediate, observationally grounded values. If an ocean model uses a 100 km grid, it requires diffusivity values on the order of $K_h \approx O(10^2 - 10^3)$ m^2s^{-1} for subgrid-scale mixing in these regions. Using a constant, non–scale-aware K_h value—or one based on small-scale processes—would severely underestimate lateral dispersion and lead to significant prediction errors, such as the unrealistic accumulation of pollutants in coastal areas and an overestimation of the time required for dilution in the open ocean.[8] Implementing scale-dependent diffusivity allows the stochastic spreading rate to dynamically adjust to the size of the particle cloud. A constant diffusivity may either overestimate or underestimate dispersion depending on the relative scale. This scale-aware parameterization is particularly critical when the particle cloud is smaller than or comparable to the model grid size, where subgrid-scale processes predominantly govern the unresolved spreading during the early stages of dispersion.

The interpretation of the derived $K_h(D)$ values requires some caution. The undrogued drifters respond to both underlying currents and surface-forcing mechanisms, including wave-induced

Stokes drift and windage.[25] From the perspective of a buoyant contaminant in the surface layer, the effective diffusivity inferred from the drifters is the relevant quantity, as such tracers experience the same combined transport. Future work combining drifter-based pair statistics with wave model output may allow for the separation of these current- and wave-driven components. While the modest deployment of 19 units in the present campaign successfully captured the theoretical small-scale dispersion regime and provided valuable first-order estimates, fully resolving the large-scale statistics requires massive cluster deployments. Such large-scale releases can be operationally facilitated by the low-cost system developed in this study, enabling the comprehensive regional mapping of $K_h(L)$ across different seasons and dynamic regimes.

Data Availability Statement

The datasets generated and analyzed during the current study are available from the corresponding author upon reasonable request.

Acknowledgments

This research was supported by Korea Institute of Marine Science & Technology Promotion (KIMST) funded by the Ministry of Oceans and Fisheries, Republic of Korea (RS-2024-00406249, RS-2022-KS221660).

References

1 S. Seo, J. M. Choi, Y.-J. Park, K. Kim, and Y.-G. Park: Mar. Pollut. Bull. **215** (2025) 117898. https://doi.org/10.1016/j.marpolbul.2025.117898
2 Y. Masumoto, Y. Miyazawa, D. Tsumune, T. Tsubono, T. Kobayashi, H. Kawamura, C. Estournel, P. Marsaleix, L. Lanerolle, A. Mehra, and Z. D. Garraffo: Elements **8** (2012) 207. https://doi.org/10.2113/gselements.8.3.207
3 S. R. Freitas, J. Panetta, K. M. Longo, L. F. Rodrigues, D. S. Moreira, N. E. Rosário, P. L. Silva Dias, M. A. F. Silva Dias, E. P. Souza, E. D. Freitas, M. Longo, A. Frassoni, A. L. Fazenda, C. M. Santos e Silva, C. A. B. Pavani, D. Eiras, D. A. França, D. Massaru, F. B. Silva, F. C. Santos, G. Pereira, G. Camponogara, G. A. Ferrada, H. F. Campos Velho, I. Menezes, J. L. Freire, M. F. Alonso, M. S. Gácita, M. Zarzur, R. M. Fonseca, R. S. Lima, R. A. Siqueira, R. Braz, S. Tomita, V. Oliveira, and L. D. Martins: Geosci. Model Dev. **10** (2017) 189. https://doi.org/10.5194/gmd-10-189-2017
4 Y. Zhou, P. Zhu, and M. Xue: J. Atmos. Sci. **74** (2017) 2639. https://doi.org/10.1175/JAS-D-16-0324.1
5 M. F. Jansen, A. Adcroft, S. Khani, and H. Kong: J. Adv. Model. Earth Syst. **11** (2019) 2844. https://doi.org/10.1029/2019MS001750
6 R. Barkan, J. C. McWilliams, A. F. Shchepetkin, M. J. Molemaker, L. Renault, A. Bracco, and J. Choi: J. Phys. Oceanogr. **47** (2017) 2325. https://doi.org/10.1175/JPO-D-17-0035.1
7 N. Ntaganou, E. P. Chassignet, and A. Bozec: J. Geophys. Res. Oceans **129** (2024) e2024JC021315. https://doi.org/10.1029/2024JC021315
8 Y. Kamidaira, H. Kawamura, T. Kobayashi, and Y. Uchiyama: J. Nucl. Sci. Technol. **56** (2019) 752. https://doi.org/10.1080/00223131.2019.1613269
9 A. Nummelin, J. J. Busecke, T. W. Haine, and R. P. Abernathey: J. Phys. Oceanogr. **51** (2021) 279. https://doi.org/10.1175/JPO-D-19-0256.1
10 I. S. Oh, V. Zhurbas, and W. Park: J. Geophys. Res. Oceans **105** (2000) 6483. https://doi.org/10.1029/2000JC900002

11 J. H. LaCasce: Lagrangian Statistics from Oceanic and Atmospheric Observations, in Transport and Mixing in Geophysical Flows, J. B. Weiss and A. Provenzale, Eds. (Springer, Berlin, 2008) pp. 165–218. https://doi.org/10.1007/978-3-540-75215-8_8
12 R. Lumpkin, T. Özgökmen, and L. Centurioni: Annu. Rev. Mar. Sci. **9** (2017) 59. https://doi.org/10.1146/annurev-marine-010816-060641
13 G. I. Taylor: Proc. London Math. Soc. **s2-20** (1922) 196. https://doi.org/10.1112/plms/s2-20.1.196
14 Y. K. Qian, S. Peng, C. X. Liang, and R. Lumpkin: J. Phys. Oceanogr. **44** (2014) 2796. https://doi.org/10.1175/JPO-D-14-0058.1
15 G. K. Batchelor: Math. Proc. Cambridge Philos. Soc. **48** (1952) 345. https://doi.org/10.1017/S0305004100027687
16 T. Meunier, P. Pérez Brunius, J. Rodríguez Outerelo, P. García Carrillo, A. Ronquillo, H. Furey, A. Ramsey, and A. Bower: J. Geophys. Res. Oceans **126** (2021) e2021JC017375. https://doi.org/10.1029/2021JC017375
17 R. Periáñez: Modelling the dispersion of radionuclides in the marine environment (Springer-Verlag, Berlin, 2005).
18 G. Novelli, C. M. Guigand, C. Cousin, E. H. Ryan, N. J. M. Laxague, H. Dai, B. K. Haus, and T. M. Özgökmen: J. Atmos. Oceanic Technol. **34** (2017) 2509. https://doi.org/10.1175/JTECH-D-17-0055.1
19 X. Y. Guo, X. H. Zhu, Y. Long, and D. J. Huang: Biogeosciences **10** (2013) 6403. https://doi.org/10.5194/bg-10-6403-2013
20 E. Van Sebille, S. Waterman, A. Barthel, R. Lumpkin, S. R. Keating, C. Fogwill, and C. Turney: J. Geophys. Res. Oceans **120** (2015) 6769. https://doi.org/10.1002/2015JC010972
21 L. Villa Castrillón, M. Ricker, J. Staneva, J. Meyerjürgens, T. H. Badewien, and E. V. Stanev: Ocean Dyn. **74** (2024) 555. https://doi.org/10.1007/s10236-024-01619-6
22 J. L. McClean, P. M. Poulain, J. W. Pelton, and M. E. Maltrud: J. Phys. Oceanogr. **32** (2002) 2472. https://doi.org/10.1175/1520-0485(2002)032<2472:EALSFS>2.0.CO;2
23 V. Zhurbas and I. S. Oh: J. Geophys. Res. **108** (2003) 3141. https://doi.org/10.1029/2002JC001596
24 S. Elipot, R. Lumpkin, R. C. Perez, J. M. Lilly, J. J. Early, and A. M. Sykulski: J. Geophys. Res. Oceans **121** (2016) 2937. https://doi.org/10.1002/2016JC011716
25 J. Röhrs, K. H. Christensen, L. R. Hole, G. Broström, M. Drivdal, and S. Sundby: Ocean Dyn. **62** (2012) 1519. https://doi.org/10.1007/s10236-012-0576-y

About the Authors

Seongbong Seo received his Ph.D. degree in oceanography from the Korea National University of Science and Technology, South Korea, in 2019. He is currently a senior research scientist at the Ocean Circulation and Climate Research Department, Korea Institute of Ocean Science and Technology. His research interests include ocean dispersion modeling and ocean vertical mixing. (sbseo@kiost.ac.kr)

Kyeong Ok Kim received his Ph.D. degree in civil engineering from Kyoto University, Japan, in 2005. He is currently a principal research scientist at the Ocean Circulation and Climate Research Department, Korea Institute of Ocean Science and Technology. His research interests include coastal hazard modelling and atmosphere-ocean interactions. (kokim@kiost.ac.kr)

Young-Gyu Park received his Ph.D. degree in physical oceanography from the Massachusetts Institute of Technology and Woods Hole Oceanographic Institution Joint Program, USA, in 1996. He is currently a principal research scientist at the Ocean Circulation and Climate Research Department, Korea Institute of Ocean Science and Technology. His research interests include large-scale ocean circulation and numerical modeling. (ypark@kiost.ac.kr)

Jun Myoung Choi received his Ph.D. degree in civil engineering from Purdue University, USA, in 2015. He is currently an associate professor in the Department of Ocean Engineering at Pukyong National University. His research interests range from the interaction between coastal structures and waves to contaminant dispersion, in situ measurements, remote sensing, and wave-flume experiments using particle image velocimetry.
(jmchoi@pknu.ac.kr)